Environment. Technology. Resources. Rezekne, Latvia
Proceedings of the 16th International Scientific and Practical Conference. 2025. Volume IV, 459-465

Numerical Experiments for the Laser Marking by Oxidation, Melting and Evaporation of AISI 304 Stainless Steel Samples

Nikolay Angelov
Department of Mathematics, Informatics and Natural Sciences
Technical University of Gabrovo
Gabrovo, Bulgaria
angelov_np@abv.bg

Lyubomir Lazov
Rezekne Academy of Riga Technical University
Rezekne, Latvia
lyubomir.lazov@rta.lv

Erika Teirumnieka
Rezekne Academy of Riga Technical University
Rezekne, Latvia
erika.teirumnieka@rta.lv

Artis Teilans
Rezekne Academy of Riga Technical University
Rezekne, Latvia
artis.teilans@rta.lv

Arturs Abolinss
Rezekne Academy of Riga Technical University
Rezekne, Latvia
artur.abolinsh@inbox.lv

***Abstract*— Theoretical numerical calculations and numerical experiments with the Temperaturfeld3D software were carried out for laser marking with a fiber laser of AISI 304 stainless steel samples. The theoretical numerical experiments are based on the interrelation of the quantities affecting the technological process, obtained from the heat conduction equation and the heat balance equation. Temperaturfeld3D is a specialized software for laser technological processes, which are characterized by small zones of influence. Temperature fields were obtained for different values of power density and speed. Graphs of the dependences of the critical power densities of melting and evaporation on the speed were constructed using both methods. Preliminary working intervals of the power density were determined for the studied speeds for laser marking by oxidation, melting and evaporation. The results obtained using both methods were compared and analysed in view of the capabilities and advantages of each of these methods.**

Keywords*— Numerical calculation, numerical experiments, laser marking, Temperaturfeld3D, AISI 304 stainless steel, power density, speed.

I. INTRODUCTION

Laser marking is a widely used technological process for creating high-quality markings on the surfaces of industrial products made of various materials, including AISI 304 stainless steel [1] – [5]. In recent decades, it has been continuously expanding its positions and gradually displacing other marking methods due to its advantages: non-contact technology, high quality, high precision, flexibility, high process efficiency, environmentally friendly process.

A number of factors influence the quality of marking [6] – [9]. For each specific case, different materials, laser sources and marking methods should be investigated to optimize the technological process. Numerical or real experiments can be performed, as well as a combination of both methods of investigation.

Some authors have investigated the laser marking process of steel through numerical experiments:

The article [10] focuses on enhancing the laser marking process for creating submillimeter-sized 2D codes on 50CrVA stainless steel. Through numerical simulations, the study examines temperature distributions during laser marking, identifying that temperature variations in the depth direction and oxidation levels in the irradiated area significantly influence the contrast of the 2D codes. The research determines optimal laser parameters, including an average laser power threshold of 3.0 W and a frequency of 100 kHz, for producing identifiable submillimeter 2D codes, aligning well with simulation results. Additionally, increasing the number of laser pulses enhances both the contrast and uniformity of the Data Matrix code modules. To improve corrosion resistance, the study finds that applying a transparent polyurethane coating effectively protects the marked codes. Finally, the research successfully demonstrates the marking of submillimeter 2D codes on cylindrical tools with a diameter of 1 mm. Overall,

Online ISSN 2256-070X
https://doi.org/10.17770/etr2025vol4.8393

the study provides a theoretical foundation and experimental approach for identifying small parts through high-quality, corrosion-resistant submillimeter laser-marked codes.

The article [11] presents the results of several numerical experiments aimed at enhancing laser marking processes on tool steel and electronic components. Utilizing specialized software developed in MATLAB, the study simulates laser marking using CuBr and Nd:YAG lasers, focusing on three different pulse durations. The numerical calculations are based on parameters derived from real-world experiments. While the article's does not detail specific findings, it emphasizes the use of simulation models to optimize laser marking techniques.

In the paper [12], the authors present the development of a proof-of-concept software designed to simulate the geometry of engraved surfaces and estimate the depth and width of engraved grooves based on associated laser parameters. The study utilizes COMSOL Multiphysics to model a moving laser beam as a heat source traversing materials such as steel, aluminum, copper, and brass. By simulating the interaction between the laser beam, operating in TEM01 mode, and these materials, the research determines the resulting temperature distributions. A key aspect of the simulation involves using COMSOL's moving mesh mode to represent material removal, which occurs when the material's temperature surpasses its vaporization point due to high-intensity laser exposure. The simulation results were validated through experimental tests, demonstrating the model's effectiveness in predicting engraving outcomes. This approach offers potential benefits in reducing setup time and material costs for laser engraving processes, especially when working with new or expensive materials.

In article [13], the authors use a mathematical model of the technological process of marking on the surface of metal products using a pulsed laser. Using the model, they obtain the optimal technological parameters for laser marking of symbols on the surface of steel products, taking into account the physical properties of the marked material. The resulting technological modes are suitable for automotive, aircraft, railway transport and for marking serial products in mechanical engineering.

The article [14] presents the development of a three-dimensional finite element method (FEM) simulation model for the nanosecond pulsed laser engraving process. The primary objective of this model is to predict the final marking area geometry of the workpiece and optimize the engraving process.

From the literature review, it can be concluded that the process of laser marking of steels has not been studied in sufficient volume, as is also true for AISI 304 steel, one of the most commonly used stainless steels in industry and households.

The aim of the publication is to investigate the technological process of laser marking with a fiber laser on AISI 304 stainless steel through theoretical numerical calculations and numerical experiments using the Temperaturfeld3D software, obtaining preliminary operating ranges of power density for different speeds using both methods and comparing the capabilities of these methods for the studied process.

II. MATERIAL AND METHODS

A. Material

AISI 304 is distinguished by its excellent corrosion resistance, very good weldability and very good mechanical properties. These are the reasons that make it one of the most widely used grades of stainless steel. Its applications are in the automotive industry, the food industry, the medical and pharmaceutical industry, construction and architecture, the chemical and petrochemical industries, and the aerospace industry. The chemical composition of the steel is presented in Table 1. It is a low-carbon steel with alloying elements chromium and nickel. Table 2 gives some basic parameters of the steel. It has low values of the coefficients of thermal conductivity and thermal diffusivity.

TABLE 1 CHEMICAL COMPOSITION OF AISI STAINLESS STEEL

Element	**Content, %**	**Element**	**Content, %**
C	< 0.08	Si	< 1.0
Cr	18.0 – 20.0	P	< 0.045
Ni	8.0 – 10.5	S	< 0.03
Mn	< 2.0	Fe	Balance

TABLE 2 BASIC PARAMETERS OF AISI 304 STAINLESS STEEL

Parameter	**Value**
Absorption capacity A	0.40
Coefficient of thermal conductivity k, W/(kg.K)	16.2
Density ρ, kg/m^3	7850
Specific heat capacity c, J/(kg.K)	500
Coefficient of thermal diffusivity a, m^2/s	4.72×10^{-6}
Melting point temperature T_m, K	1700
Vaporization temperature T_v, K	2950
Latent heat of melting L_m, kJ/kg	266
Latent heat of evaporation L_v, kJ/kg	6500

B. Laser system

Numerical experiments were performed for a laser technology system with a fiber laser. It has very good repeatability, very high positioning accuracy and the ability to move the laser beam in a very wide range. Fiber laser has radiation with a wavelength in the infrared region. It has extremely high beam quality and high efficiency. Table 3 gives the main parameters of the laser system.

TABLE 3 SOME PARAMETERS OF LASER SYSTEM FOR MARKING

Parameter	**Value**
Wavelength λ, nm	1064

Power *P*, W	20
Diameter of work spot *d*, μm	30
Efficiency, %	40
Speed, mm/s	< 6000
Positioning accuracy, μm	2.5

C. Software

To perform the numerical experiments, the Temperaturfeld3D program is used. It is the working environment for calculating temperature fields with a wide range of input parameters and options for analyzing and storing the calculated results. After selecting the dynamic model (suitable for the laser marking process), the main window opens (see Fig. 1). From it, the user has access to the three main sections of the software – input/output, model parameters, calculation.

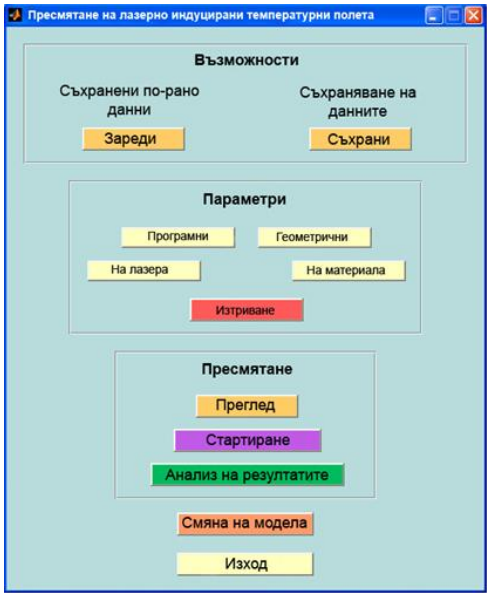

Fig. 1. Main window of the Temperaturfeld3D program.

Input data includes: program parameters, geometric parameters, laser parameters, and material parameters.

After starting and performing the calculations to obtain the temperature fields in the impact zone, the output results are obtained, which include: maximum temperature profile, temperature profile of the material at a given time, temperature dependence on time, temperature change in the depth of the material, animation of the entire process, approximation of the results.

D. Metods

The determination of preliminary operating ranges of power density for different speeds for the laser marking process can be performed both by numerical calculations with expressions giving the relationship between the quantities affecting the process and by numerical experiments with specialized software for studying the process. The obtained results are compared and thus it can be determined which of the two methods is more suitable for these studies.

- Theoretical numerical calculations

Power density and speed are the main parameters affecting the laser marking process of steel. From the heat conduction equation and the heat balance equation, a relationship can be obtained between power density, speed and temperature in the impact zone.

For the critical power density of melting, the formula is obtained

$$q_{scm} = \frac{(1+s)k(T_m - T_0)}{2A}\sqrt{\frac{\pi v}{ad}} \qquad (1)$$

where k is the thermal conductivity coefficient, a – thermal diffusivity coefficient, A – absorption capacity, d – diameter of the working spot, T_0 – initial temperature, $s = \frac{L_m}{c(T_m - T_0)}$ (2) is a parameter, L_m – specific heat of melting, c – specific heat capacity.

The formula for the critical power density of evaporation is

$$q_{scv} = \frac{(1+s')k(T_v - T_0)}{2A}\sqrt{\frac{\pi v}{ad}} \qquad (3)$$

where $s' = \frac{L_m + L_v}{c(T_m - T_0)}$ (4) is a parameter, L_v – specific heat of evaporation.

The determination of the intervals of change of the power density for oxidation, melting and evaporation occurs in three stages:

- Calculation of the critical power density of melting q_{scm} and evaporation q_{scv}.

The values of the critical power densities of melting for different speeds are determined by formulas (1) and (2), with the speed changing in a interval from 10 mm/s to 100 mm/s. The values of the critical evaporation power densities for different speeds are determined by formulas (3) and (4). Graphs of the dependences of the critical power density of melting on speed and the critical power density of evaporation on speed are drawn.

2) Determination of the maximum power density q_{smax} for the laser used.

The maximum power density q_{smax} is calculated using the formula

$$q_{smax} = \frac{4P_{max}}{\pi d^2} \qquad (5)$$

where P_{max} is the maximum power of the laser.

3) Determination of the preliminary power density intervals for oxidation, melting and evaporation for the selected laser and material

The results are presented in a suitable table. The first column shows different speeds, the second column contains the power density intervals for oxidation, the third column for melting, the fourth for evaporation. The third and fourth columns show the power density intervals. These intervals are clearly shown in the graphical images. The oxidation zone is below the graph of the dependence of the critical melting power density on the speed. The melting zone is between the two graphs. The evaporation

zone is above the graph of the dependence of the critical power density of evaporation on the velocity and is limited from above by the maximum laser power density.

- Numerical experiments with the program Temperaturfeld3D

In order to obtain the preliminary operating intervals of power density for different speeds for laser marking by oxidation, melting and evaporation, a series of numerical experiments were carried out with the Temperaturfeld3D program. The difference in this case compared to the calculations using the above formulas is the consideration of the temperature change during the process of some input parameters such as absorption capacity, coefficient of thermal conductivity and density of the material.

Numerical experiments are performed in several stages:

- Obtaining the temperature dependence of power density for different speeds

Through numerical experiments, the temperature fields in the impact zone are obtained for different power densities and speeds (a total of 80 calculations with the Temperatutfeld3d program). From each temperature field, the maximum temperature of the material surface is determined. Graphs of the temperature dependence on the power density are drawn for different speeds. From these, the critical power densities of melting and evaporation are determined for each of the studied speeds;

- Drawing graphs of the dependence of the critical power density of melting and evaporation on the speed;
- Determination of preliminary working intervals for the laser marking process by oxidation, melting and evaporation.

- Comparing the results obtained by the two methods

On one coordinate system, the graphs of the dependence of the critical power density of melting on the speed, obtained from the results of numerical calculations and numerical experiments, are drawn. On another coordinate system, the graphs of the dependence of the critical power density of evaporation on the speed, obtained from the results of numerical calculations and numerical experiments, are drawn. The results obtained by the two methods are analysed and compared.

III. Results and Discussion

Numerical calculations and numerical experiments were carried out according to the presented methodology.

A. Theoretical numerical calculations

Numerical calculations were performed to determine the critical power density of melting and evaporation for different speeds according to formulas (1) – (4). The speed varied in the range from 10 mm/s to 100 mm/s in increments of 10 mm/s. From the results obtained, graphs of the dependences of the critical power densities of melting and evaporationon speeds were constructed (see Fig. 2). The following conclusions can be drawn from them:

- A nonlinear dependence of the two critical power densities on the speed is obtained, as the critical power densities increase with increasing speed;
- The critical power density of melting varies from 0.058×10^{10} W/m^2 to 0.185×10^{10} W/m^2 for the entire studied speed interval. The critical power density of evaporation varies from 0.690×10^{10} W/m^2 to 1.544×10^{10} W/m^2 for the entire studied speed interval;
- Three zones are observed:

zone (1) – corresponds to oxidation of the material;
zone (2) – corresponds to melting of the material;
zone (3) – corresponds to evaporation of the material.

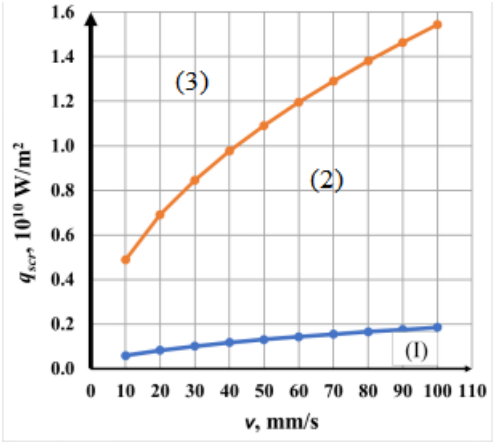

Fig. 2. Graphs of the dependence of the critical power density of melting (blue graph) and evaporation (orange graph) on the speed.

For the maximum power density according to formula (5) it was obtained $P_{max} = 2.831\times10^{10}$ W/m^2.

Based on the obtained calculation results, preliminary operating intervals of power density for different speeds for laser marking by oxidation, melting and evaporation were obtained (see Table 4).

TABLE 4 PRELIMINARY OPERATING INTERVALS OF POWER DENSITY FOR DIFFERENT SPEEDS FOR THE LASER MARKING PROCESS

v, mm/s	**q_s, W/m^2**		
	Oxidation	*Melting*	*Evaporation*
10	$< 0.058\times10^{10}$	0.058×10^{10} – 0.488×10^{10}	0.488×10^{10} – 2.831×10^{10}
20	$< 0.083\times10^{10}$	0.083×10^{10} – 0.690×10^{10}	0.690×10^{10} – 2.831×10^{10}
30	$< 0.101\times10^{10}$	0.101×10^{10} – 0.846×10^{10}	0.846×10^{10} – 2.831×10^{10}
40	$< 0.117\times10^{10}$	0.117×10^{10} – 0.976×10^{10}	0.976×10^{10} – 2.831×10^{10}
50	$< 0.131\times10^{10}$	0.131×10^{10} – 1.092×10^{10}	1.092×10^{10} – 2.831×10^{10}
60	$< 0.143\times10^{10}$	0.143×10^{10} – 1.196×10^{10}	1.196×10^{10} – 2.831×10^{10}

v, mm/s	q_s, W/m²		
	Oxidation	*Melting*	*Evaporation*
70	$< 0.155\times10^{10}$	$0.155\times10^{10} – 1.292\times10^{10}$	$1.292\times10^{10} – 2.831\times10^{10}$
80	$< 0.165\times10^{10}$	$0.165\times10^{10} – 1.381\times10^{10}$	$1.381\times10^{10} – 2.831\times10^{10}$
90	$< 0.175\times10^{10}$	$0.175\times10^{10} – 1.465\times10^{10}$	$1.465\times10^{10} – 2.831\times10^{10}$
100	$< 0.185\times10^{10}$	$0.185\times10^{10} – 1.544\times10^{10}$	$1.544\times10^{10} – 2.831\times10^{10}$

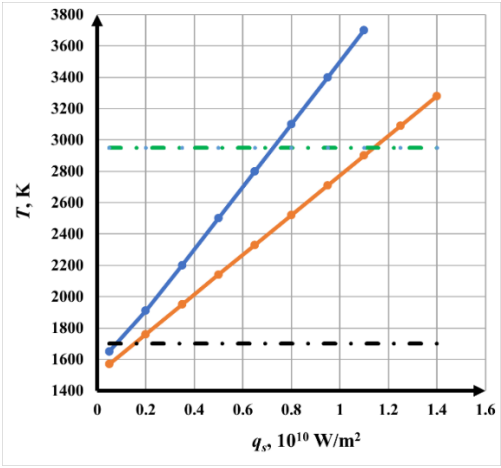

Fig. 3. Graphs of the dependence of temperature on power density for speeds: 30 mm/s – blue graph and 70 mm/s – orange graph.

B. -Numerical experiments with the program Temperaturfeld3D

A series of numerical experiments were performed to study the process of laser marking of AISI 304 stainless steel samples with a fiber laser. Temperature fields in the impact zone were obtained for different power densities and different speeds. The speed varied in the interval from 10 mm/s to 100 mm/s with a step of 10 mm/s. The temperature dependences on the power density for different speeds were obtained. The Figure 3 shows two graphs of the temperature dependence on the power density for speeds: 30 mm/s – blue graph and 70 mm/s – orange graph. From the constructed graphs, the critical power density of melting for speeds 30 mm/s and 70 mm/s is determined from the intersection points of the black line with the blue and orange lines. From the intersection points of the green line with the blue and orange lines, the critical power densities of evaporation for these speeds are obtained. In a similar manner, the critical power densities of melting and evaporation are determined for the remaining studied velocities.

At the next stage, graphs of the dependence of the critical power density of melting and evaporationon the speed were drawn (see Fig. 4). From the analysis of the graphs it follows:

- With increasing speed, the critical power densities increase, as the dependence is nonlinear;
- The critical melting power density changes from 0.056×10^{10} W/m² to 0.174×10^{10} W/m² for the entire studied speed interval. The critical power density of evaporation changes from 0.468×10^{10} W/m² to 1.451×10^{10} W/m² for the entire studied speed interval;
- The same three zones are observed for the laser marking process as in the results of numerical calculations.

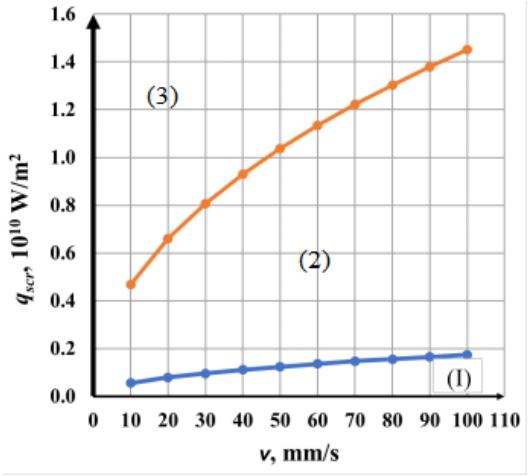

Fig. 4. Graphs of the dependence of the critical power density of melting (blue graph) and evaporation (orange graph) on the speed

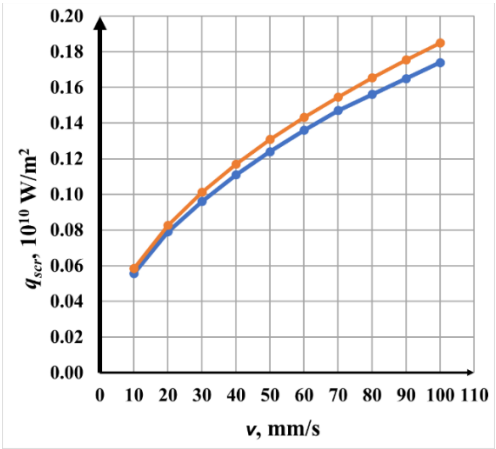

Fig. 5. Graphs of the dependence of the critical melting power density on the speed: blue graph – from numerical experiments and orange graph – from numerical calculations

The obtained preliminary operating intervals of power density for different speeds for laser marking by oxidation, melting and evaporation are presented in Table 5.

TABLE 5 PRELIMINARY OPERATING POWER DENSITY INTERVALS FOR DIFFERENT SPEEDS FOR THE LASER MARKING PROCESS

v, mm/s	q_s, W/m^2		
	Oxidation	*Melting*	*Evaporation*
10	$< 0.056\times10^{10}$	0.056×10^{10} – 0.468×10^{10}	0.468×10^{10} – 2.831×10^{10}
20	$< 0.079\times10^{10}$	0.079×10^{10} – 0.660×10^{10}	0.660×10^{10} – 2.831×10^{10}
30	$< 0.096\times10^{10}$	0.096×10^{10} – 0.807×10^{10}	0.807×10^{10} – 2.831×10^{10}
40	$< 0.111\times10^{10}$	0.111×10^{10} – 0.930×10^{10}	0.930×10^{10} – 2.831×10^{10}
50	$< 0.124\times10^{10}$	0.124×10^{10} – 1.037×10^{10}	1.037×10^{10} – 2.831×10^{10}
60	$< 0.136\times10^{10}$	0.136×10^{10} – 1.134×10^{10}	1.134×10^{10} – 2.831×10^{10}
70	$< 0.147\times10^{10}$	0.147×10^{10} – 1.222×10^{10}	1.222×10^{10} – 2.831×10^{10}
80	$< 0.156\times10^{10}$	0.156×10^{10} – 1.303×10^{10}	1.303×10^{10} – 2.831×10^{10}
90	$< 0.165\times10^{10}$	0.165×10^{10} – 1.380×10^{10}	1.380×10^{10} – 2.831×10^{10}
100	$< 0.174\times10^{10}$	0.174×10^{10} – 1.451×10^{10}	1.451×10^{10} – 2.831×10^{10}

C. Comparing the results obtained by the two methods

According to the methodology, graphs of the dependence of the critical power density of melting on the speed (see Fig. 5) are drawn, obtained from the results of theoretical numerical calculations (orange graph) and numerical experiments with the Temperaturfeld3D program (blue graph). It can be seen that for the numerical calculations the values of the critical power density are about 4.0 – 6.0 % higher than those from the numerical experiments. The graphs of the dependence of the critical power density of evaporation on the speed are presented in Fig. 6. Again, the values of the critical power density of evaporation from the numerical calculations are higher than those from the numerical experiments, differing by about 4.2 – 6.0 %. The explanation is that in the Temperaturfeld3D program the temperature dependence of some parameters is set. For example, as is known, with increasing temperature the absorption capacity of metals and alloys increases, in particular the investigated AISI 304 stainless steel.

It should be noted that achieving the results with numerical experiments using the Temperaturfeld3D program requires a lot of time. A large number of numerical experiments are carried out (at least 80 experiments as noted in the methodology) and the obtained temperature fields are analyzed, a large number of graphs are drawn and analyzed until the preliminary working intervals of the power density for laser marking by oxidation, melting and evaporation are obtained. To obtain the same preliminary working intervals using theoretical numerical calculations, a small number of calculations are made according to the formulas from the theory. These calculations can be automated using a calculator created, for example, in the Excel program. Two graphs are drawn and analyzed in one coordinate system. Therefore, in this case, the time to obtain the final results is several times less.

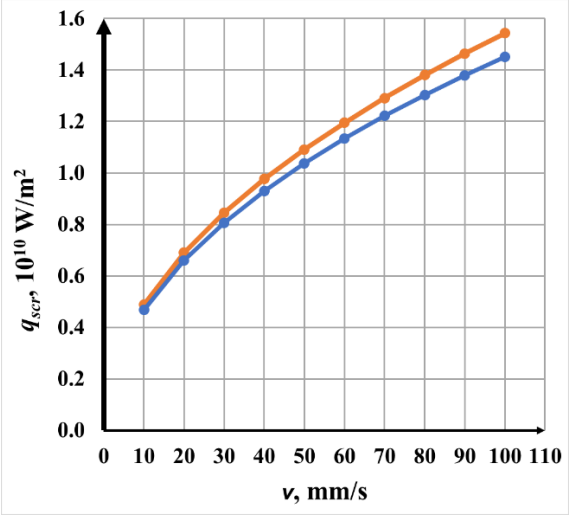

Fig. 6. Graphs of the dependence of the critical power density of evaporation on the speed: blue graph – from numerical experiments and orange graph – from numerical calculations

The accuracy of the results obtained with the Temperaturfeld3D program is slightly higher (4.0 – 6.0 % difference in the obtained results). Both proposed methods have a place in the research for obtaining the preliminary working intervals of the power density for different speeds, but the method with numerical calculations is more direct and saves a lot of time for the researchers.

IV. CONCLUSIONS

This study investigated the laser marking of AISI 304 stainless steel through oxidation, melting, and evaporation using theoretical numerical calculations and numerical experiments conducted with Temperaturfeld3D software. By analysing the interrelation of key process parameters derived from the heat conduction and heat balance equations, the study provided insights into the thermal behaviour of the material under different laser power densities and scanning speeds.

The following results were achieved:

- temperature fields were obtained for different power densities and speeds;
- graphs of the dependence of the critical power density of melting and evaporation on the speed were constructed by both methods;
- preliminary working intervals of the power density were determined for the studied speeds for laser marking by oxidation, melting and evaporation by both research methods.

The comparison between theoretical calculations and numerical simulations highlighted the strengths and limitations of each method, demonstrating their complementary roles in predicting process outcomes.

Overall, this study demonstrates the effectiveness of using FEM-based simulation models to predict and enhance the laser marking process. The results contribute to a deeper understanding of laser-material interactions in stainless steel marking processes, providing valuable guidelines for optimizing laser parameters. Future research could focus on experimental validation of the findings and further refinement of numerical models to improve accuracy and applicability in industrial settings.

REFERENCES

[1] B. Gu, Review: 40 years of laser-marking industrial applications, Lasers and Applications in Science and Engineering, 2006, San Jose, California, United States, Proceedings, Volume 6106, Photon Processing in Microelectronics and Photonics V, 610601, 2006, https://doi.org/10.1117/12.640838

[2] L. Morawiski, S. Swillo and A. Kosanda, Application of Laser Barcode Technology to Sheet Metal Parts Identification, Scientific paper of Silesian University of Technology, Organization and Management Series, No. 162, 2022, http://dx.doi.org/10.29119/1641-3466.2022.162.27

[3] T. Kyrychok, O. Nazarenko and O. Korotenko, Eds., Determining the influence of technological parameters of the laser processing of plastic cards edges on improving their wear resistance, Eastern-European Journal of Enterprise Technologies, Vol. 6, No. 1 (132), 2024, DOI: 10.15587/1729-4061.2024.317448

[4] C. Patel, A. Patel and R. Patel, A Review on Laser Marking Process for Different Materials, IJSRD - International Journal for Scientific Research & Development| Vol. 5, Issue 1, 2017,| ISSN (online): 2321-0613

[5] R. Hamid, A. Marjan, H. Heikki and S. Antti, Color Laser Marking: Repeatability, Stability and Resistance Against Mechanical, Chemical and Environmental Effects, IEEE Access, 2020, DOI: 10.1109/ACCESS.2020.3040744

[6] A. Schkutowa and T. Frick, Laser color marking of stainless steel – Investigation of the fluence dependent and thermal mechanisms in generating laser induced surface modifications, 13th CIRP Conference on Photonic Technologies, 15-19 September 2024, Fürth, Germany, Procedia CIRP 124, 661–664, 2024

[7] E. Amara and H. Fadhela, Experimental investigations on fiber laser color marking of steels, Applied Surface Science, 351, May 2015, DOI:10.1016/j.apsusc.2015.05.095

[8] L. Sobotova and M. Badida, Laser marking as environment technology, Open Engineering, ol. 7, No. 1, pp. 303-316, 2017, https://doi.org/10.1515/eng-2017-0030

[9] Y. Geng, J. Li and C. Lu, Experimental and numerical investigations on color stability of laser color marking, Optics and Lasers in Engineering, Volume 159, 107225, December 2022, https://doi.org/10.1016/j.optlaseng.2022.107225

[10] X. Li, L. Yang and B. Changz, Eds., Simulation and process optimization for laser marking of submillimetre rasterizing 2D code on stainless steel, International Journal of Modern Physics B, Vol. 34, No. 28, 2050266, pp. 1-18, 2020, DOI: 10.1142/S0217979220502665

[11] L. Lazov and N. Angelov Petrov, Optimization of laser marking with the help of simulation models, Turkish Journal of Physics, 37(1):145-150, January 2013, DOI: 10.3906/fiz-1202-4

[12] H. Karbasi, COMSOL Assisted Simulation of Laser Engraving, Engineering, Materials Science, Physics , Proceedings of the COMSOL Conference 2010 Boston, pp. 1-10, 2010

[13] O. Ganzulenko and A. Petkova, Simulation and approbation of the marking laser process on metal materials, IOP Publishing, Journal of Physics: Conference Series 1753, 012016, 2021, DOI:10.1088/1742-6596/1753/1/012016

[14] E. Nikolidakis and A. Antoniadis, FEM modeling simulation of laser engraving, The International Journal of Advanced Manufacturing Technology, 105:3489–3498, 2019, https://doi.org/10.1007/s00170-019-04603-3